IOP Publishing Superconductor Science and Technology
Supercond. Sci. Technol. 31 (2018) 065008 (9pp) https://doi.org/10.1088/1361-6668/aabb4b

Clustered atom-replaced structure in single-crystal-like metal oxide

Takeshi Araki[1], Mariko Hayashi[1], Hirotaka Ishii[1], Daisaku Yokoe[2], Ryuji Yoshida[2], Takeharu Kato[2], Gen Nishijima[3] and Akiyoshi Matsumoto[3]

[1] Corporate Research and Development Center, Toshiba Corporation, 1 Komukai-Toshiba-cho, Saiwai-ku, Kawasaki 212-8582, Japan
[2] Nanostructures Research Laboratory, Japan Fine Ceramics Center, 2-4-1 Mutsuno, Atsuta-ku, Nagoya, 456-8587, Japan
[3] Research Center for Functional Materials, National Institute for Materials Science, 3-13 Sakura, Tsukuba-shi, 305-0003, Japan

E-mail: takeshi2.araki@toshiba.co.jp

Received 18 January 2018, revised 22 March 2018
Accepted for publication 3 April 2018
Published 2 May 2018

Abstract

By means of metal organic deposition using trifluoroacetates (TFA-MOD), we replaced and localized two or more atoms in a single-crystalline structure having almost perfect orientation. Thus, we created a new functional structure, namely, clustered atom-replaced structure (CARS), having single-crystal-like metal oxide. We replaced metals in the oxide with Sm and Lu and localized them. Energy dispersive x-ray spectroscopy results, where the Sm signal increases with the Lu signal in the single-crystalline structure, confirm evidence of CARS. We also form other CARS with three additional metals, including Pr. The valence number of Pr might change from 3+ to approximately 4+, thereby reducing the Pr–Ba distance. We directly observed the structure by a high-angle annular dark-field image, which provided further evidence of CARS. The key to establishing CARS is an equilibrium chemical reaction and a combination of additional larger and smaller unit cells to matrix cells. We made a new functional metal oxide with CARS and expect to realize CARS in other metal oxide structures in the future by using the above-mentioned process.

Keywords: TFA-MOD, cluster, clustered atom-replaced structure, quasi-liquid network model, YBCO, superconductor

(Some figures may appear in colour only in the online journal)

1. Introduction

Single-crystalline-like metal oxide films have recently been prepared for various applications, including solar power, dielectric films and superconductors. Many groups have attempted to dope other materials in the oxide films or prepare additional structures in them, in order to endow the materials with additional properties. However, the doped atoms or additional layers cause inhomogeneity, which causes non-uniformity, instability and low reproducibility. To avoid these influences, a perfectly oriented structure is desirable. This prompts the question: how can the properties be improved while maintaining such a perfectly oriented structure?

Improving the properties of metal oxide in a perfectly oriented structure will necessarily involve replacing the metals in the oxide. If only one metal is replaced, the replaced metal generally has a lattice constant of the unit cell different from that of the matrix atoms. Consequently, the replaced metal will be ultimately dispersed. In some cases, it may be possible to exploit such a structure in order to improve the properties. However, a localized area having replaced atoms is desirable in most cases. Could two or more atoms be replaced, while maintaining the perfectly oriented structure?

We found that the key to achieving the structure is liquid-phase growth and volumetric anisotropy. Metal organic deposition using trifuoroacetates [1, 2] (TFA-MOD) is one of the processes for yielding perfectly oriented metal oxide having a perovskite structure. This process has a liquid growth mode. The quasi-liquid [3] enables us to obtain a perfectly aligned structure with the following mode. The quasi-liquid presumably

means a liquid phase exists during the firing process, but we have obtained no direct evidence of this yet. The quasi-liquid, which contains at least yttrium (or rare earth metals), barium, copper, oxygen, hydrogen and fluorine, yields or accommodates $YBa_2Cu_3O_{7-x}$ and hydrogen fluoride in the equilibrium state during the firing process. In TFA-MOD, by choosing the process conditions, a newly grown unit cell can be achieved only on a cube-on-cube site. If a unit cell is to grow in the off-axis direction, as indicated by the green rectangles in figure 1(A), off-axis growth can be suppressed by choosing the conditions at the minimum energy level to grow the oriented structure. Only a strongly connected unit cell grows, as indicated by the red rectangles in figure 1(A). The off-axis unit cell will revert to the quasi-liquid without growing [4]. With this special growth mode, highly oriented metal oxide is routinely obtained by TFA-MOD [5].

The growth mode with quasi-liquid in TFA-MOD suggests how CARS might be realized. We simultaneously add both larger and smaller unit cells to the matrix layer to realize CARS. Matrix cells mostly grow on the former layer. As the matrix layer grows, the concentration of metals with larger or smaller unit cells in the local area increases. At a certain moment, a larger unit cell may grow on the former matrix layer. The grown larger unit cell and matrix underlayer make a narrow space, which stimulates growth of a smaller unit cell. Such growth must be realized by providing the minimum energy, as discussed above, in regard to TFA-MOD. Based on the scientific background, larger and smaller unit cells are grown and localized in perfectly oriented metal oxide. We report the study and results of CARS in a single-crystal-like structure.

2. Methods

We prepared three kinds of coating solution. The basic coating solution is for $YBa_2Cu_3O_{7-x}$. The other two coating solutions are prepared by substituting Y with Sm, Lu, Pr and Tm. First, we describe the preparation process for $YBa_2Cu_3O_{7-x}$. 99.99% Y-acetate, 99.99% Ba-acetate and 99.994% Cu-acetate are dissolved into distilled and deionized water in 1.00:2.00:3.00 metal ratios to yield a blue transparent solution. Stoichiometric trifluoroacetic acid is added to the solution to realize a light blue transparent solution. The solution is refined to realize a transparent blue gel, which is dissolved into plenty of dehydrated 99.5% methanol to realize a methanol coating solution having water impurities and acetic acid of about 5% [6]. The coating solution with impurities is refined again to realize a blue gel, which mostly confines methanol inside instead of water. By resolving the blue gel, which has methanol, into dehydrated methanol, we obtained a highly purified coating solution. We have already reported the method elsewhere as the solvent-into-gel method for obtaining a purified coating solution [7]. The total volume of the coating solution is 20 ml. The metallic concentration of the highly purified coating solution is 1.50 mol l^{-1}.

The coating solution for $Y_{0.8}Sm_{0.1}Lu_{0.1}Ba_2Cu_3O_{7-x}$ is obtained by the same method. We only substituted 20% Y-acetate with 10% Sm-acetate and 10% Lu-acetate as starting salts. The coating solution for $Y_{0.92}Pr_{0.02}Sm_{0.02}Tm_{0.04}Ba_2Cu_3O_{7-x}$ is also obtained by the above method.

Uniform gel film was obtained by spin-coating on 10 mm square or 10×28 mm $LaAlO_3$ single crystals with an acceleration time of 0.4 s and a spinning rate of 4000 rpm for 120 s [8] or with an acceleration time of 0.2 s and a spinning rate of 2000 rpm for 120 s. The resulting films were 150 nm (4000 rpm) and 220 nm (2000 rpm) in thickness, respectively. The thickness of $(Y_{0.8}Sm_{0.1}Lu_{0.1})Ba_2Cu_3O_{7-x}$ film was 150 nm and that of $(Y_{0.92}Pr_{0.02}Sm_{0.02}Tm_{0.04})Ba_2Cu_3O_{7-x}$ film 220 nm. The obtained gel film was quickly settled into a calcining furnace and calcined with the calcining profile shown in figure 10 of reference [4] to become a translucent brown precursor film with a microstructure consisting of CuO nanocrystallites and Y-Ba-O-F amorphous matrix. The 10–20 nm size grains are CuO nanocrystallites and the other areas are a Y-Ba-O-F amorphous matrix. The precursor film was soft and easily peeled away from the substrate. However, the precursor film was chemically very stable in air even with a high level of humidity because the precursor film is well-oxidized material and could not be changed chemically. The precursor film was fired and annealed with the profile shown in figure 12 of reference [4] to become YBCO perovskite-type oxide film.

X-ray diffraction (XRD) measurements were used to characterize the epitaxial nature of the films having CARS. The obtained $(Y_{0.8}Sm_{0.1}Lu_{0.1})Ba_2Cu_3O_{7-x}$ film was prepared using focused ion beam to be thin film by an external vendor. The vendor observed the film by means of a cross-sectional transmission electron microscopy (TEM) image and the result is shown in figure 4. Energy dispersive x-ray spectrometry (EDS) signals of Sm and Lu were measured for the prepared film by the vendor from ten 5 nm square areas. Since the strongest Sm peak is hindered by Ba signal, we evaluate the second-strongest Sm signal and the strongest Lu signals in figure 5. All the other high-angle annular dark-field (HAADF) images and line profiles were measured at the Japan Fine Ceramics Center.

The films with CARS on the $LaAlO_3$ substrate were thinned in a Hitachi NB5000 focused ion beam scanning electron microscope system equipped with a micro-sampling system for the preparation of TEM and scanning transmission electron microscopy specimens. In addition, the cross-sectional specimens were further thinned using a Gatan PIPS ion milling system at the accelerating voltage of 1–0.5 kV to remove the focused ion-beam-damaged layers formed on the TEM specimen [9]. The specimen was examined in a JEM-2100F (JEOL Ltd) with a spherical aberration corrector at the accelerating voltage of 200 kV. HAADF images were recorded with a 73–194 mrad detector.

We prepared four separated silver electrodes on 10×28 mm $YBa_2Cu_3O_{7-x}/LaAlO_3$ films by physical vapor deposition at 300 K under vacuum condition at 0.1 Pa. The sample was fixed on a measuring probe for J_c measurement by the four-probe method in a high magnetic field at the National Institute of Materials Science. We firmly set the measuring samples on the probe and enveloped the sample entirely. The samples were cooled by 4.2 K helium gas.

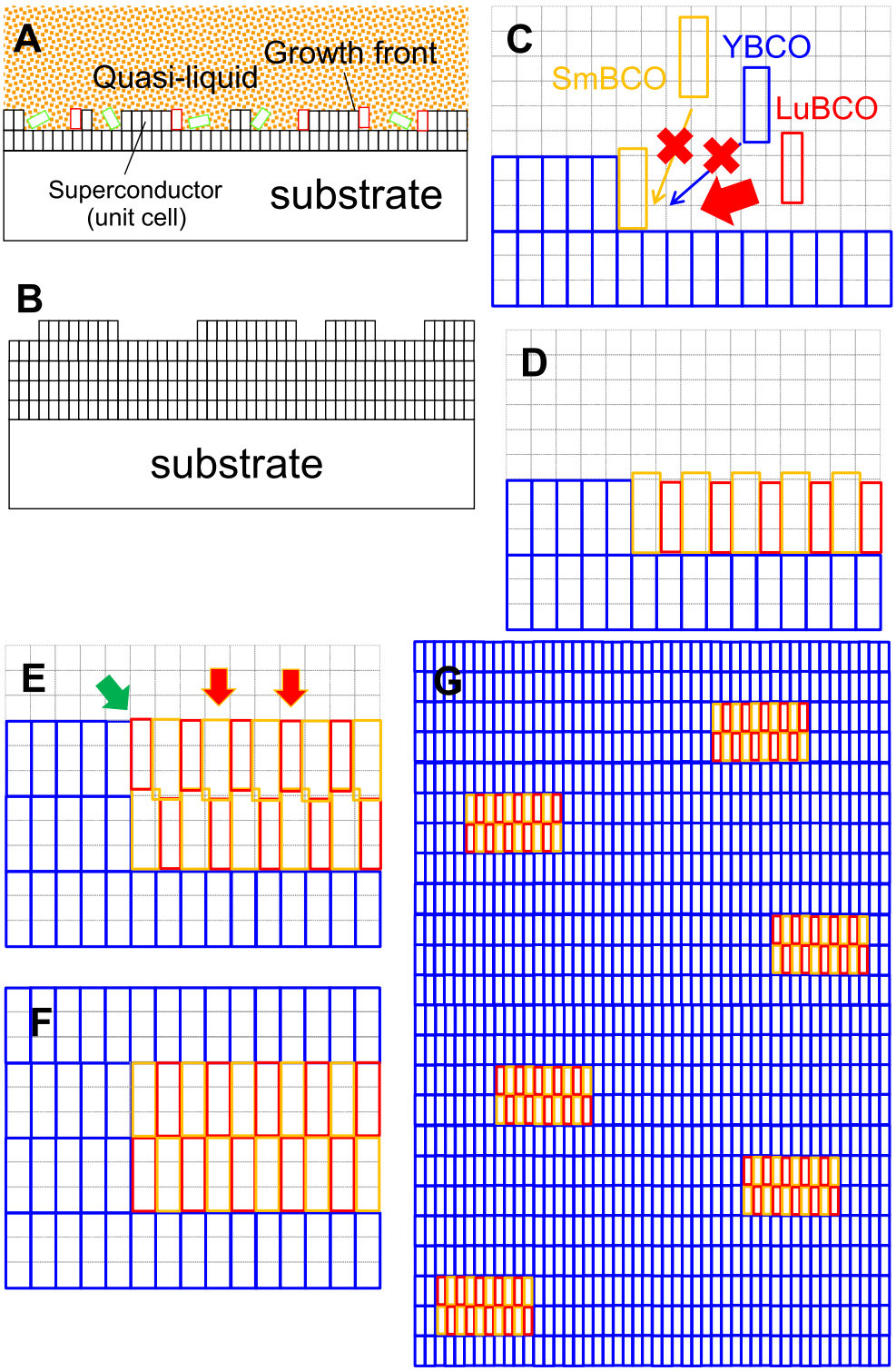

Figure 1. (A) Schematic illustration of quasi-liquid network during firing process. (B) After firing process, isolated quasi-liquid forms islands. (C) Grown larger unit cell causes growth of smaller unit cell in adjacent site. (D) Large and small unit cells form the first layer. (E) Clustered atom-replaced structure (CARS) and matrix occasionally form a small gap indicated by a green arrow. (F) On the disk-like structure of CARS, matrix units have a strong possibility for growth. (G) Illustration of metal oxide structure having CARS. Periodically dispersed CARS structure forms in metal oxide.

The probe was set inside a variable temperature insert, which was set underground. We could increase the magnetic field *c*-axis orientation of the perovskite structure. The maximum direct current was 100 A. The maximum measuring time to 125% value of critical current (100%/4 s) was 5 s to evaluate the inner uniformity by suppressing heating on the silver electrode. The critical current was determined by 1 microvolt per centimeter, which is standard in the superconducting field.

3. Results and discussion

3.1. The quasi-liquid model implies the possibility of CARS

Prior to explaining the above growth scheme, we explain the growth mode of conventional metal organic deposition (MOD). The general MOD process has a solid-phase growth mode. MOD requires oxygen, hydrogen and metals for the starting material to form the oxide film. It is difficult to prepare a well-aligned structure by means of this solid growth. In solid growth mode, a grown off-axis unit cell can never be removed. Once an off-axis unit cell forms, it causes random orientation growth. Therefore, it is difficult for MOD processes to yield a well-aligned structure on a wide area. On the other hand, as discussed above, TFA-MOD has a special growth mode during the firing process. The quasi-liquid is formed by metals, oxygen, hydrogen and fluorine [3]. The only difference between TFA-MOD and MOD is the fluorine atom. However, the fluorine atom plays a great role in yielding a perfectly oriented structure at the atomic level. The fluorine atom makes quasi-liquid at lower temperature. In TFA-MOD, from the results of a fluorine detector, the quasi-liquid appears at around 773 K and, from XRD results, a well-aligned structure can be formed at around 1000 K.

The quasi-liquid forms in the whole calcined film during the firing process and such quasi-liquid phases connect with one another as if a quasi-liquid network forms, as shown in figure 1(A). An aligned metal oxide (perovskite) unit cell is released onto the last layer and simultaneously hydrogen fluoride gas is also released. We can easily control the process conditions, such as the firing temperature, humidity and oxygen partial pressure, to permit further growth only for the cube-on-cube structure (red rectangle) in figure 1(A). The green rectangle never grows and melts back to the quasi-liquid. The hydrogen fluoride gas is immediately dissolved into the quasi-liquid. The creation of both the unit cell and hydrogen fluorine gas depends on an equilibrium chemical reaction. What is interesting is that the dominant chemical reaction yields quasi-liquid, not metal oxide. However, such a tendency works well to form a perfectly oriented structure. When one hydrogen fluoride molecule is removed from the quasi-liquid, one oxide structure forms on the growth front. This gradual growth scheme facilitates the yield of a perfectly oriented structure [4], as shown in figure 1(B). A rough surface typical of the TFA-MOD-derived growth scheme appears.

3.2. The first evidence of CARS

Here, we define the $YBa_2Cu_3O_{7-x}$ unit cell as Y-U. Y can be replaced with rare earth metals, such as Sm or Lu. We prepared Y-U film including 10% Sm-U and 10% Lu-U (80% Y-U) on $LaAlO_3$ singe-crystal substrate and measured the XRD. The results are shown in figure 2(A) and the detail of the results is shown in figure 2(B). Figure 2(A) shows only $LaAlO_3$ substrate and YBCO(00n) peaks. Intensities of the YBCO(00n) exhibit a tendency, namely, the intensity of YBCO(001) is generally weaker than that of YBCO(002). On the other hand, the peak intensity of SmBCO(002) is much stronger than that of SmBCO(001) [10]. LuBCO exhibits the same tendency as SmBCO. Figure 2 shows that SmBCO and LuBCO influence the tendency of the YBCO film to some extent. The film has 10% SmBCO and 10% LuBCO. If the SmBCO unit cell existed separated from the YBCO unit cells, the influence of SmBCO would be observed. However, figure 2(B) only shows YBCO tails at around 46.53° at the SmBCO(006) peak. The results confirm the single-crystal-like structure. We observed the film by TEM. Shown in figure 3 is an image of the film captured by TEM. From the image, we could not recognize the difference between matrix Y-U and CARS (Sm-U and Lu-U). The contrast of the image indicates different directions of unit cells. In TFA-MOD, the direction of one nucleus is not the same as that of another. Growth areas from two nuclei are connected at a point and form a low-angle grain boundary. The grain boundary appears as the contrast designated with white arrow in figure 3. The film must have CARS of Sm-U and Lu-U. However, we could not recognize any influenced structure. The cancellation system discussed above might conceal CARS.

To detect CARS, we measured EDS signals in a 5 nm square area. If Sm and Lu atoms are clustered in the film and the 5 nm square area shows stronger Sm signal than its average, Lu signal must also be stronger than its average.

The results are plotted in figure 4. We measured Sm and Lu signals from ten 5 nm square areas. Here, since Ba signal has a large influence on the strongest Sm signal, we use the Sm second-strongest signal. Figure 4 shows the strong relationship from nine data out of ten. The tendency implies the formation of CARS. This is the first evidence of CARS.

However, we could not determine the approximate size of the clustered area from figure 4 and wanted to obtain direct evidence of CARS. To confirm the existence of CARS, we decided to create a bent structure in the perfectly oriented unit cells and to obtain the evidence of direct observation by means of the following method.

3.3. Direct observation of CARS by HAADF

A possible atom for the bent structure is Pr, which is known to form perovskite structure with Ba and Cu. However, the oxide of Pr-U has no superconductivity at 4.2 K in liquid helium [11, 12]. Among the lanthanide metals that form perovskite structure at Y-site, Pr is the only atom to show no superconductivity. We presume that the absence of superconductivity may derive from the changed chemical nature of Pr. The valence number of Pr in its ionic state is 3+ or 4+. Perovskite structure indirectly shows the valence number of 3+. We assume the valence number of Pr in fired film at lower temperature such as 4.2 or 77. 4 K is around 4+ [12].

Perovskite structure of $YBa_2Cu_3O_{7-x}$ ($X = 0.07$) has both low-occupation and high-occupation oxygen sites. Here, Y has the valence number of 3+. If the valence number of Pr

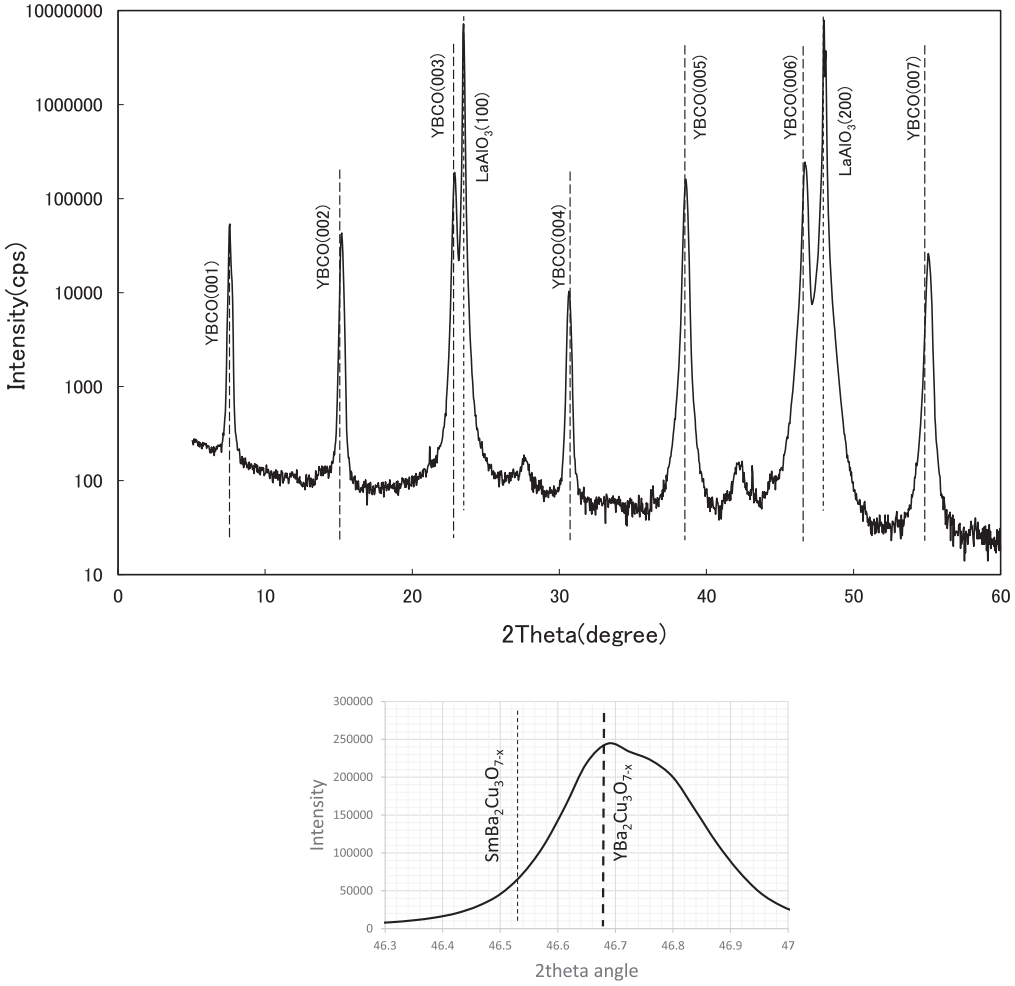

Figure 2. ((A), upper) XRD result. Only $LaAlO_3$ substrate and YBCO (00n) peaks are observed. ((B), lower) Detailed figure at around 46.68° showed the single peak result.

changes from 3+ to about 4+, the number of oxygens in $PrBa_2Cu_3O_{7-x}$ may change from 6.93 to about 7.43. The valence number of Pr may not be strictly 4.00+ and may be 3.96, 3.99, and so on. However, here we simplify the discussion by assuming the valence number of 4.00 for Pr. In the case of Pr^{4+}, the former low-oxygen-occupation site is occupied with additional oxygens. The oxygen site is adjacent to a Cu^{2+} site. If the oxygen site is vacant, a repulsion force is generated by two Cu^{2+} sites. On the other hand, if the additional oxygen is provided to the former vacant site, an attractive force between Cu^{2+} and O^{2-} is generated. A-axis and *C*-axis of Pr-U should be shorter than those of the original Pr-U. In addition to the effect of increased oxygen, the ionic diameter of Pr becomes smaller with the valence number change. Eight-coordinate Pr^{3+} and eight-coordinate Pr^{4+} ions have diameters of 1.266 and 1.10 Å, respectively [13]. The shrink ratio from Pr^{3+} to Pr^{4+} is −13.1%. This large shrink force causes no superconductivity in $PrBa_2Cu_3O_{7-x}$ ($x = -0.43$). $PrBa_2Cu_3O_{7-x}$ has perovskite structure at firing temperature of around 1073 K. At that temperature, Pr^{3+} has a large ionic diameter. If the ratio of Pr is only 2% or 4% in volumetric content, a large cage of the lattice is formed at 1073 K, but the valence number change of Pr makes an attractive force locally. In such a case, two Ba presumably move to the Pr site. As discussed above regarding figure 1(F), CARS may be a disk-like structure. In the structure, the distance between one Ba in a larger unit cell and another Ba in a smaller unit cell might be longer than that before moving. To detect the expanded Ba-Ba structure, we observed images of $(Pr_{0.02}Sm_{0.02}Tm_{0.04}Y_{0.92})Ba_2Cu_3O_{7-x}$ film by HAADF.

Typical images are shown in figures 5(A) and (B). Figure 5(A) shows the normal area. Two lines of bright dots and dark dots in the horizontal direction indicate Ba and Y, respectively. Cu exists between Y and Ba or between Ba and Ba in the vertical direction. Fine periodic structure is observed in figure 5(A). On the other hand, in figure 5(B), broadened Ba-Ba areas are indicated by a red-line rectangle and normal Ba-Ba areas by a broken-orange-line rectangle.

We measured line profiles of figures 5(A) and (B), which are summarized in figures 6(A) and (B). We recognized the

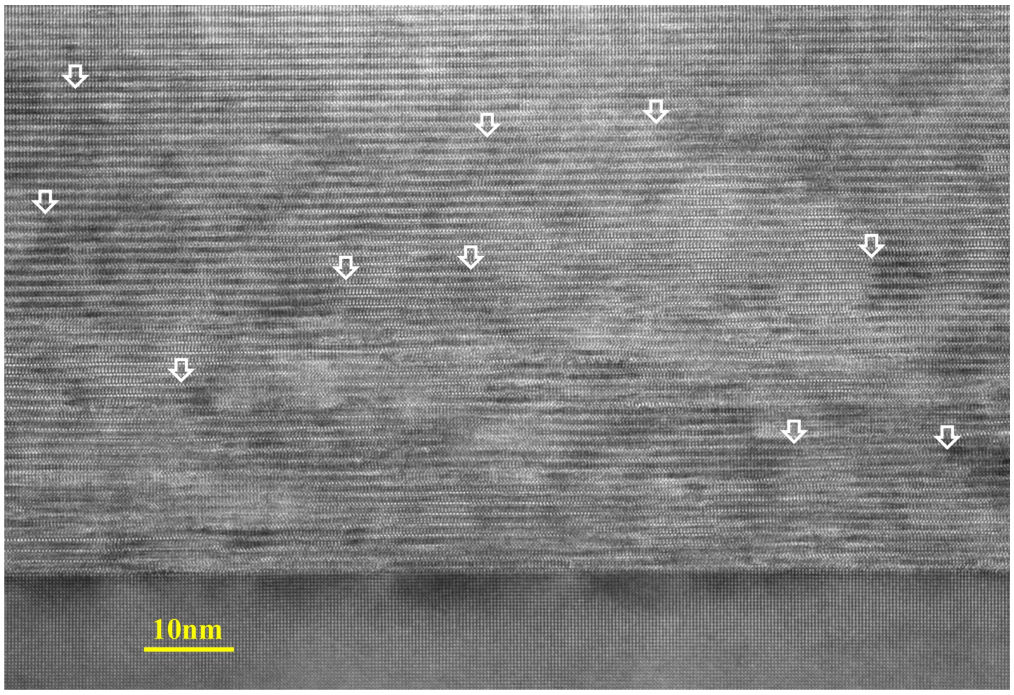

Figure 3. TEM image of YBCO with CARS, including Sm and Lu. Two nucleated unit cells and the growth area connected with the low-angle grain boundary appear as bright or dark areas, indicated by white arrows in this figure. Although the perfectly oriented area has CARS having Sm and Lu, the cancellation system hinders the grain boundary between CARS and the matrix.

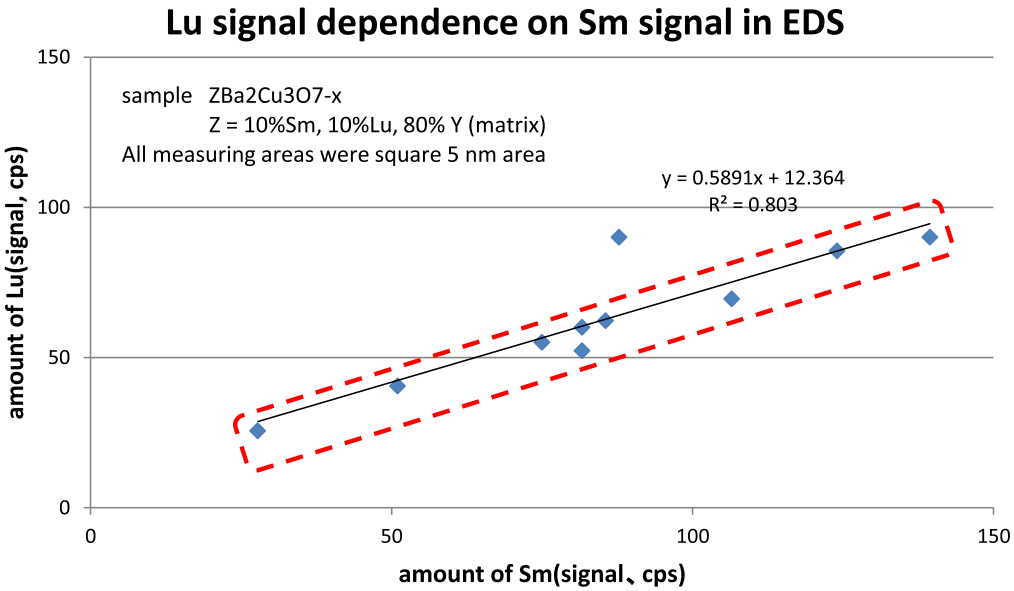

Figure 4. Lu signal dependence on Sm signal in the EDS map. We measured ten data in the 5 nm square areas of figure 3. Nine out of ten data show apparent dependence. This dependence is evidence of CARS.

periodic structure in figure 6(A). On the other hand, we discovered two broader areas in Ba-Ba sites in figure 6(B). This result shows the disk-like structure discussed in regard to figure 1(F). From figure 6(B), Ba-Y-Ba length is 0.71 nm and longer than that of Ba-Y-Ba in figure 6(A). This may be attributable to the change in the chemical nature of Pr. As discussed above, Pr^{3+} must have a larger ionic diameter at 1073 K. Therefore, the total length of Ba-Ba-Y-Ba is longer than that in figure 6(A). The total lengths are 1.14 (6 A) and 1.17 (6B) nm, respectively. The initial length of Ba-Ba is presumably the same as that in figures 6(A), 0.44 nm. In the case of the initial state, the length of Ba-Pr-Ba must be 0.73 nm (1.17–0.44). The length of Ba-Pr-Ba shrinks from 0.73 to 0.71. The length data indirectly support the evidence of CARS.

We could also obtain other evidence that the Pr valence may change the disk-like structure in figures 6(A) and (B). If CARS forms only the disk-like structure shown in figure 1(F), the average position of Y-site in the lower layer goes downwards as a result of the change of Pr valence, because

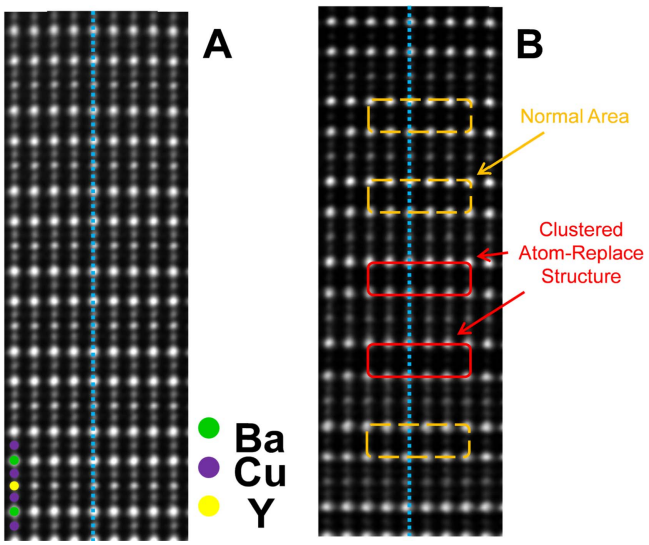

Figure 5. (A) HAADF image of a normal area. We could recognize the periodic structure of two Ba, one Y and three Cu lines. Brightest dots show Ba and the second-brightest dots show Y. (B) HAADF image of CARS area. Normal areas are indicated by a broken-orange-line rectangle and two CARS areas are indicated by a red-line rectangle. Both kinds of rectangle have the same length in the vertical direction. Width was narrower in the case of the red line than the orange line. This is also evidence of CARS.

Pr-U shrinks, but the others do not shrink. Then, the average position of Pr goes downwards slightly, and Pr-Cu distance seems smaller than that in the normal state shown in figure 6(A). In the case of the upper layer, the same phenomenon occurs and the average position of Y-site goes upwards slightly. The two purple lines on the right in figure 6(B) indicate the Cu position. The position changes slightly upwards, which is predicted in light of the above discussion. On the other hand, the two purple lines on the left go in the opposite direction slightly. Figure 6(B) apparently shows the two-layered structure of CARS.

So far, we have not been able to confirm CARS by Pr-U, Y-U and single small M-U (Tm-U, Yb-U or Lu-U). CARS having Pr needs Sm-U assistance. The reason has yet to be clarified in detail. CARS must be formed by volumetric anisotropy. Pr^{3+} might be very large to form CARS. We could only confirm CARS in the case of mixed Pr with Sm as large atoms.

If the chemical reaction were dominant in terms of yielding metal oxide, rapid growth would doubtlessly cause disorder in the structure formed, because such rapid growth would never permit the repairing system discussed above. With this scheme, a perfectly oriented metal oxide layer would be obtainable on even a 500 m long metal tape with high reproducibility [5, 14]. As discussed above, by choosing the process we provide the minimum energy to grow only a cube-on-cube structure with high reproducibility.

Profound understanding of the quasi-liquid model [4] provides a further possibility of establishing CARS.

Cell volume and cell length of M-U follow the lanthanide shrinkage rule [11]. Cell length c is assumed to be in the following order: U(Pr) > U(Sm) > U(Y) > U(Tm) > U(Lu). Here, U(Pr) means the size of cell length c of Pr-U. We discuss the formation of clustered Sm-U and Lu-U structure in Y-U matrix, as illustrated in figure 1(C). Matrix Y-U will be predominant and easily grows on the substrate or on the last Y-U layer. As growth of Y-U proceeds, consumption of Y increases the concentration of Sm and Lu in the local area of the quasi-liquid. Finally, at a certain moment, a larger unit cell of Sm-U may grow onto the growth front, as shown in figure 1(C). Of course, a smaller unit cell of Lu-U has the possibility to grow on the site. Here, we discuss only one case of Sm-U. Since the Sm-U has a larger lattice constant, the edges of the Sm-U and Y-U matrix in the underlayer provide the narrower space shown in figure 1(C). If we provide minimum energy by choosing the process conditions, the narrow space will only accept Lu-U growth.

This growth mode is also efficient in the front and rear areas. After forming the first clustered atoms, the surface of both these areas is rough, as shown in figure 1(D). Small Lu-U is easily grown onto Sm-U, as shown in figure 1(E), because of volumetric anisotropy in the vertical direction. However, total lengths in the vertical direction of Sm-U (lower) + Lu-U (upper) and Lu-U + Sm-U are the same. A flat surface will appear on the two-layered clusters shown in figure 1(E). Therefore, the formation of a two-layered structure will be strongly encouraged. Although the edge area indicated by the green arrow might have a small step, this gap seems not to stimulate Sm-U or Lu-U growth. On the flat plane, the matrix of Y may grow. Consequently, the disk-like structure is basically enveloped with the matrix area, as shown in figure 1(F). If Sm-U and Lu-U are entirely enveloped by matrix Y-U, the center position will be withdrawn equally in the upper and lower directions. Therefore, from the centerline it seems as if only Y-U exists. This cancellation system will conceal the existence of CARS from TEM observation.

We can detect the two-layered structure by means of HAADF line profiles, as discussed in the following section.

3.4. Innumerous uniformly dispersed CARS in the film

We observed the atomic arrangements of the film by HAADF and one of the results is shown in figure 5. The figure presents at least ten CARS marked with yellow lines. Lengths are from 6.4–9.1 nm. The length is not diameter, but apparent size. If the two-layered CARS has disk-like structure, the edge of the disk will be difficult to see. If the column is 10 nm in diameter and the thickness of the observed area is 20 nm, the center area can easily be seen. However, we can only see 5 nm thickness at the edge of the column. In this case, the signal from CARS is only one-fourth. We may hardly see the signal. Based on this assumption, the apparent diameter must be $\frac{\sqrt{3}}{2}$ of the original diameter in the case of perfect columnar structure. If the hypothesis is correct, the diameters of the CARS are from 7.4–10.5 nm. From figure 5, we could observe similar diameters. The reason is easily understood in light of the following growth model. From figure 7, the CARS appear to be located mainly in the area on the right, but it depends on sample preparation. We sliced film in the inclined

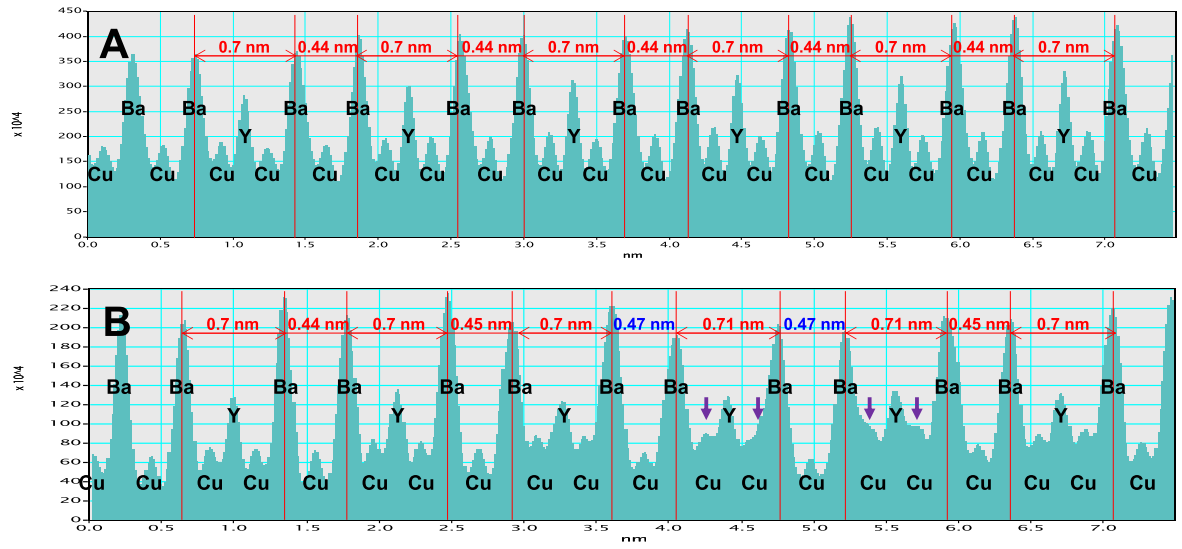

Figure 6. (A) Line profile of signals of figure 5(A). Periodic structure was confirmed from the distance. (B) Line profile of signals of figure 5(B). Two unit cells in the center area were influenced by CARS. Distance of Ba-Ba line is 0.47 nm, which is apparently wider than the others. Distance of Ba-Y(site)-Ba line is also broad. Detailed explanation is provided in the main text.

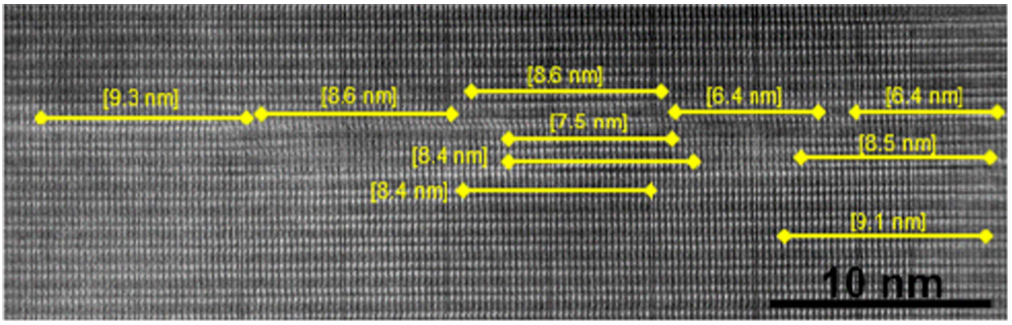

Figure 7. CARS directly observed by HAADF. CARS of similar sizes are observed. CARS with similar diameter are dispersed all over the films.

direction to see the image of a thick area where we could detect CARS as discussed above. There appear to be few CARS in the thick area.

Matrix atoms are predominant in this film. Therefore, matrix atoms have the largest possibility to nucleate first. As we discussed regarding the quasi-liquid network model, by providing energy just for the film, matrix atoms grow next to the formed matrix. As the matrix grows, the concentration of large or small atoms increases. Finally, large or small atoms nucleate and CARS forms. However, the formation of CARS decreases the concentration of large or small atoms. Then matrix atom starts growing again. This cycle will continue from the bottom to the top of the film. Consequently, uniformly dispersed CARS is formed. We obtained innumerous uniformly dispersed CARS in the film, which is schematically illustrated in figure 1(G).

3.5. Improved superconducting properties in magnetic field by CARS

The film observed in figure 7 has CARS. The diameter of CARS seems to be 8 or 9 nm. One-fourth of the CARS is non-superconducting $PrBa_2Cu_3O_{7-x}$. The average potential of CARS in the superconducting state will be at least approximately 75%, only if the Pr site is not a superconductor. This structure works as a pinning center for magnetic vortex and improves superconducting properties in a magnetic field. To confirm the effect, we measured superconducting properties of the two films; one has the same structure as that shown in figure 7, and the other is pure $YBa_2Cu_3O_{7-x}$ without CARS. The results shown in figure 8 apparently show the improvement of the superconductivity in a magnetic field. Lower temperature and lower magnetic field are particularly effective for improvement. Although the reason is unclear at present, we expect to clarify it in the near future.

The improvement of superconductivity in a magnetic field is the third evidence of CARS. From three independent results, we have undoubtedly established CARS in metal oxide.

In this report, we demonstrate the CARS in perovskite structure. Profound understanding of the quasi-liquid network model enables us to achieve a novel and more efficient structure. In the near future, we expect to achieve the same CARS in other oxide structures. We expect to realize the structure by volumetric anisotropy and the quasi-liquid growth mode.

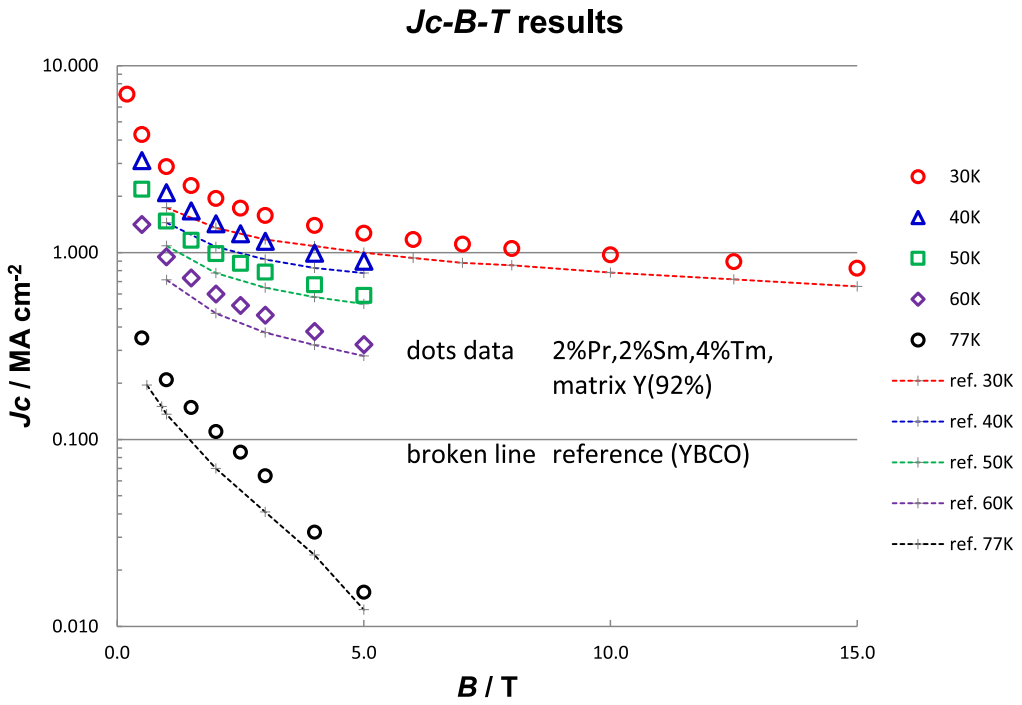

Figure 8. Critical current densities of YBCO with CARS and without CARS in a magnetic field. Critical current density of YBCO with CARS apparently increases at low temperature and low magnetic field. Since CARS having Pr has less superconducting potential, magnetic flux is pinned within the CARS area. This is also evidence of CARS.

4. Conclusions

In summary, we realized CARS in metal oxide. CARS has both perfectly oriented structure and localized clustered atom area. CARS can be realized by the combination of liquid growth and volumetric anisotropy. Volumetric anisotropy could be caused by the presence of both larger and smaller unit cells in the matrix. In other words, CARS required at least two kinds of metal.

We made CARS having Sm and Lu clustered structure at Y-site of $YBa_2Cu_3O_{7-x}$. The obtained CARS is confirmed by EDS results, where Sm intensity increases with that of Lu from nine of ten measuring points.

We also made CARS having three replaced metals, one of which was Pr. The valence number of Pr seems to change from 3+ to approximately 4+. The change causes broader Ba-Ba bonds and the bonds are directly detected in a HAADF image. This is the second evidence of CARS.

CARS including Pr is 7–10 nm in width and 2.4 nm in height (two layers). Since one-fourth of CARS is Pr, which has no superconducting region, $YBa_2Cu_3O_{7-x}$ superconductor having CARS must have excellent superconducting properties in a magnetic field. We also confirmed the results, which is the third evidence of CARS.

CARS can theoretically be formed in metal oxide using liquid growth mode and volumetric anisotropy. Although this paper is the first demonstration of CARS, in the near future, we intend to form CARS in other oxide structures. This technology undoubtedly improves the properties of metal oxide and opens a new scientific field.

ORCID iDs

Takeshi Araki https://orcid.org/0000-0003-1107-7786
Mariko Hayashi https://orcid.org/0000-0001-6005-5829

References

[1] Gupta A, Jagannathan R, Cooper E I, Giess E A, Landman J I and Hussey B W 1988 *Appl. Phys. Lett.* **52** 2077
[2] McIntyre P C, Cima M J and Roshko A 1995 *J. Appl. Phys.* **77** 5263
[3] Araki T, Niwa T, Yamada Y, Hirabayashi I, Shibata J, Ikuhara Y, Kato K, KatoT and Hirayama T 2002 *J. Appl. Phys.* **92** 3318
[4] Araki T and Hirabayashi I 2003 *Supercond. Sci. Technol.* **16** R71
[5] Rupich M W *et al* 2010 *Supercond. Sci. Technol.* **23** 014015
[6] Araki T, Yamagiwa K, Hirabayashi I, Suzuki K and Tanaka S 2001 *Supercond. Sci. Technol.* **14** L21
[7] Araki T 2004 *Bull. Chem. Soc. Jpn.* **77** 1051
[8] Araki T, Kurosaki H, Yamada Y, Hirabayashi I, Shibata J and Hirayama T 2001 *Supercond. Sci. Technol.* **14** 783
[9] Sasaki H *et al* 2004 *J. Electron Microsc.* **53** 497
[10] Araki T and Hirabayashi I 2005 *Jpn. J. Appl. Phys.* **44** L1138
[11] Tarascon J M, McKinnon W R, Greene L H, Hull G W and Vogel E M 1987 *Phys. Rev.* B **36** 226
[12] Akhavan M 2002 *Physica.* B **321** 265
[13] Shannon R D 1976 *Acta Cryst.* **A32** 751
[14] Sim K, Kim S, Cho J, Jang H and Hwang S 2013 *IEEE Trans. Appl. Supercond.* **23** 5401804